# Reports

## Protein Electron Transfer Rates Set by the Bridging Secondary and Tertiary Structure

D. N. BERATAN, J. N. BETTS,* J. N. ONUCHIC

**The rate of long-distance electron transfer in proteins rapidly decreases with distance, which is indicative of an electron tunneling process. Calculations predict that the distance dependence of electron transfer in native proteins is controlled by the protein's structural motif. The helix and sheet content of a protein and the tertiary arrangement of these secondary structural units define the distance dependence of electronic coupling in that protein. The calculations use a tunneling pathway model applied previously with success to ruthenated proteins. The analysis ranks the average distance decay constant for electronic coupling in electron transfer proteins and identifies the amino acids that are coupled to the charge localization site more strongly or weakly than average for their distance.**

MANY BIOLOGICAL ELECTRON transfer reactions involve charge transport over considerable distance (>5 Å). Therefore, electron tunneling occurs through the protein, and the rate of transport is proportional to the square of the electronic coupling between donor and acceptor species (*1*). We recently developed a tunneling pathway model for electron transfer in proteins that identifies the dominant bonding and nonbonding interactions responsible for the donor-acceptor coupling (*2*). The model successfully predicts the relative rates of electron transfer in ruthenated cytochrome c, myoglobin, and cytochrome $b_5$. In the cytochrome c and $b_5$ derivatives, order of magnitude rate differences between isomers with nearly identical transfer distances were successfully explained with the pathway model (*3*).

In weakly coupled donor-acceptor systems, the rate of electron transfer is

$$k_{ET} = \frac{2\pi}{\hbar} |T_{DA}|^2 (F.C.) \quad (1)$$

where $T_{DA}$ is the electronic tunneling matrix element between donor and acceptor localized states and (F.C.) is the Franck-Condon factor determined by the activated (or tunneling) nuclear processes coupled to the transport. A physical tunneling pathway is defined as a combination of interacting bonds that link donor with acceptor. Segments of the pathway are characterized as covalent (*C*), hydrogen-bonded (*H*), or through-space (*S*), depending on whether the bonds share a common atom (*C*), are linked by a hydrogen bond (*H*), or are in van der Waals contact (*S*). The pathway model assumes that noninteracting tunneling pathways dominate $T_{DA}$, and the numerical implementation of the model seeks those dominant paths (*3*). The contribution to the donor-acceptor electronic coupling mediated by an individual physical tunneling pathway is as follows (*2*):

$$\frac{\beta_A \beta_D \beta_1}{(E - \alpha_L^1)(E - \alpha_R^1) - \beta_1^2} \prod_{i=2}^{N_C} \epsilon_i^C \prod_{j=1}^{N_S} \epsilon_j^S \prod_{k=1}^{N_H} \epsilon_k^H \quad (2)$$

where $\alpha_L^1$ and $\alpha_R^1$ are the orbital energies of the two hybrid atomic orbitals in the first bond of the pathway, and the subscripted values of β are coupling matrix elements between orbitals at the chain ends (*2, 3*). The energy of the tunneling electron is *E*.

We recently implemented a graph-search algorithm to determine the dominant tunneling pathways in proteins and to calculate their relative electronic couplings. The following values of the decay parameters in Eq. 2 were used (*3*):

$$\epsilon^C = 0.6 \quad (3a)$$

$$\epsilon^H = 0.36 \times \exp[-1.7(R - 2.8)] \quad (3b)$$

$$\epsilon^S = 0.6 \times \exp[-1.7(R - 1.4)] \quad (3c)$$

The distances, *R*, are in angstroms, and the decay factors, ε, are unitless (*4*). We estimated the through-bond decay factor by using data from existing model compounds and protein electron transfer rates. We calculated the through-space decay factor, 1.7 $Å^{-1}$, using the known typical binding energies for the localized states, and the H bond decay factor arises from approximating the H bond as two stretched covalent bonds (*2, 3*). The parameterization neglects bond type differences, but for mapping the residues in proteins that mediate tunneling and estimating relative couplings, this method is adequate. Differences in the ε values for various bond types are small enough that this approximation is adequate for these initial calculations. In fact, the nature of the predicted pathways is insensitive to the details of the parameters if they are chosen in a physically realistic range. The model explains a substantial amount of experimental data that are inconsistent with simpler single exponential decay expressions for $T_{DA}$ (*3*). Typically only a few viable pathways or families of pathways exist because of the relatively weak interaction between nonbonded groups.

Earlier estimates of coupling matrix elements in proteins relied on the calculation of tunneling barrier heights based on optical properties or electronic structure calculations on simplified systems (*5*). More recently, strategies that treat details of the polypeptide electronic structure have been under study (*3, 6*). The pathway search method outlined above is apparently the first to allow global searches from a single center (for example, Cu atom, Fe-S cluster, or metalloporphyrin) to every other (nonhydrogen) atom in the protein. These searches are possible because of the relative simplicity of the model. The calculation is broken into two phases. First, bonded and nonbonded connections within a radius (usually 6 Å) of each atom are identified and their coupling is calculated. Local through-space connections are eliminated if stronger bonded links exist between the atoms. More than half of the computing time is spent establishing and screening the local connections. The connection-coupling list is used by the program to seek pathways between the donor and acceptor that maximize the product in Eq. 2.

An expanding set of experimental data is now emerging for electron transfer in proteins between residues at fixed distances. Surface modification with transition metal complexes, chemical modification of chromophores in multisubunit proteins, site-directed mutagenesis, and semisynthesis have provided a wide variety of electron transfer proteins with

D. N. Beratan, Jet Propulsion Laboratory, California Institute of Technology, Pasadena, CA 91109, and The Beckman Institute, California Institute of Technology, Pasadena, CA 91125.
J. N. Betts, Jet Propulsion Laboratory, California Institute of Technology, Pasadena, CA 91109.
J. N. Onuchic, Department of Physics, University of California, San Diego, La Jolla, CA 92093.

*Present address: Woods Hole Oceanographic Institute, E34-201, Woods Hole, MA 02139.

**Table 1.** Best fits of pathway couplings to $\exp[-(\beta/2)R_{DA}]$. Distances in heme proteins are measured to the closest atom in the porphyrin ring. The 95% confidence limits on $\beta/2$ are $\pm 0.03$ Å$^{-1}$. The standard deviation of the decay length fit for each protein is $\sigma$ (*9*). The structures were taken from the Brookhaven Protein Data Bank coordinate files of *Pseudomonas* cytochrome $c_{551}$ (351c and 451c), sperm whale myoglobin (1mbo and 5mbn), Bovine cytochrome $b_5$ (2b5c), albacore cytochrome c (3cyt and 5cyt), *Chromatium* high-potential Fe protein (1hip), *Alcaligenes* azurin (2acu, some residue data not available), and poplar plastocyanin (1pcy and 5pcy). Values of $\beta/2$ for the oxidized and reduced structures of a single protein (for cytochrome c and plastocyanin) differ by no more than 0.01 Å$^{-1}$. The same is true of $\beta/2$ in oxymyoglobin and deoxymyoglobin.

| Protein | $\beta/2$ (Å$^{-1}$) | $\sigma$ ($\beta/2$) | Helix (%) | Sheet (%) |
|---|---|---|---|---|
| Cytochrome $c_{551}$ | 0.76 | 0.22 | 51 | |
| Cytochrome $b_5$ | 0.73 | 0.22 | 57 | 29 |
| Myoglobin | 0.71 | 0.22 | 79 | |
| Cytochrome c | 0.61 | 0.21 | 51 | |
| HiPIP | 0.60 | 0.16 | 11 | 16 |
| Azurin | 0.55 | 0.16 | 14 | 47 |
| Plastocyanin | 0.49 | 0.19 | 5 | 62 |

known bridging structures (*7*) to which this method can be applied.

For tunneling through a structureless one-dimensional barrier between localized vibronic states, the rate is

$$k'_{ET} = A^2 \exp(-\beta R_{DA})(\text{F.C.}) \qquad (4)$$

where $R_{DA}$ is the donor-acceptor distance and the tunneling matrix element is $T_{DA} = A \exp(-R_{DA}\beta/2)$. Experimental data from a variety of proteins with different donors and acceptors are often fitted to this expression to estimate $\beta$. The barrier height is determined by the redox potentials of the donor and acceptor and the electronic structure of the protein. To connect our method with this common formulation of the rate, and to calculate the average decay length resulting from the pathway analysis of a specific protein, we calculated the best fit exponential decay constant for $T_{DA}$ using the couplings calculated with the pathway model. The pathway coupling for a specific metalloprotein was calculated between the transition metal site and every other nonhydrogen atom in the protein (846 sites in albacore cytochrome c). Myoglobin, cytochrome c, cytochrome $c_{551}$, cytochrome $b_5$, high-potential iron protein (HiPIP), azurin, and plastocyanin were examined (*8*). We fitted the single exponential expression for each protein, using the largest pathway coupling found between the native charge localization site and each other nonhydrogen atom (correlation coefficients ~0.85 to 0.90). The atomic positions were fixed at the crystallographic coordinates. The matrix element decay factor $\beta$ was found to be protein-dependent; the results appear in Table 1. The variation in $\beta$ arises simply from connectivity differences in the proteins. This effect is distinct from others that might arise from differences in the electron tunneling energy or the atom types and hybridization between proteins (*5*). The pathways are calculated from the point in the heme ring edge nearest to the target atom, from the Cu site to the target atom, or from the Fe-S cluster to the target atom (the HiPIP values are averages of eight independent sets of searches from each atom in the Fe-S cluster).

The values chosen for $\epsilon^C$ (0.6) and the through-space decay factor (1.7 Å$^{-1}$) in Eq. 3 determine the maximum and minimum possible values for $\beta$; coupling can decay no faster than it would decay purely through space and no more slowly than it would if there were a fully extended bonded chain between donor and acceptor. For a covalent chain, $\epsilon^C = 0.6$ generates $\beta/2 = 0.42$ Å$^{-1}$ (we assume tetrahedral atoms). The calculated pathway-mediated values of $\beta/2$ vary from 0.76 to 0.49 Å$^{-1}$, or 73 to 95% of the bond-mediated value.

The marked difference between the heme and blue Cu protein distance dependence arises from secondary and tertiary structure differences. One can understand this difference by examining the atoms that are especially strongly or weakly coupled (for their distance) in the proteins. The ratio ($\zeta_N$) of the largest pathway coupling to site $N$ to the coupling calculated with the average value of $\beta/2$ fitted for that specific protein, identifies sites that are more strongly or more weakly coupled than average for their distance.

$$\zeta_N = \frac{\prod_i \epsilon_i}{A \exp[-R_{DN}\beta/2]} \qquad (5)$$

Atoms with $\zeta_N > 1$ are called "hot" spots, and those with $\zeta_N < 1$ are called "cold" spots. Maps of $\zeta_N$ and the pathway couplings appear in Fig. 1. In the heme proteins, the smallest values of $\zeta_N$ are found for amino acid atoms in mid-helix, and the largest values of $\zeta_N$ occur for amino acids directly coupled to the porphyrin or near turns between helical segments. In the blue Cu $\beta$-barrel proteins, $\beta$ strands coordinated to the Cu have many atoms with $\zeta_N > 1$ in the entire strand, and the ratio is generally somewhat less than one

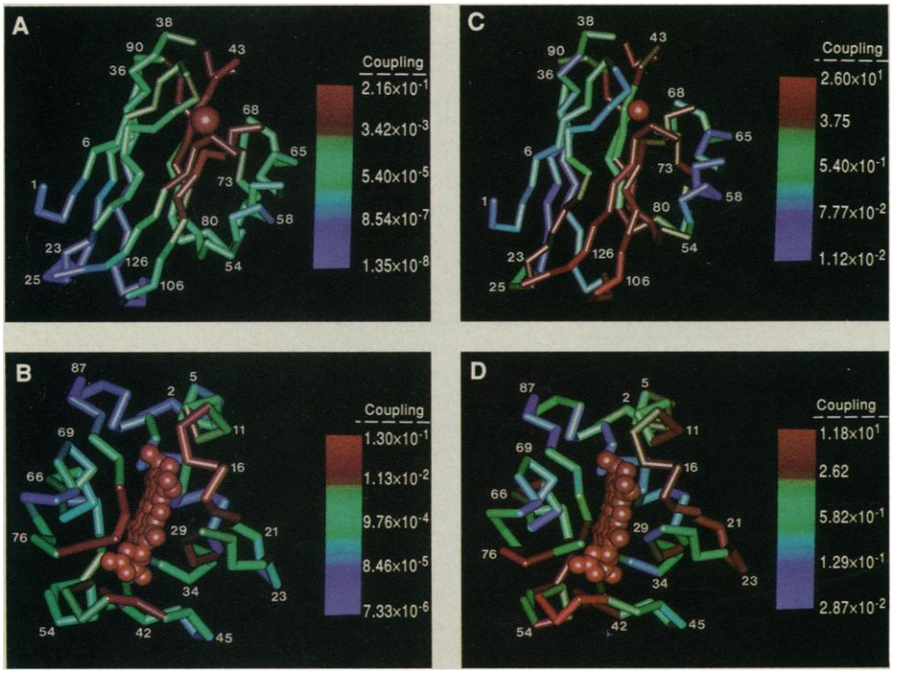


**Fig. 1.** Labeled traces of the $\alpha$-carbons in azurin (**A**) and cytochrome c (**B**) showing the strength of the pathway coupling (Eq. 5 numerator only) to the blue Cu or heme sites (red signifies strong coupling, blue weak, and green intermediate), which decays approximately exponentially with distance. Also shown are the sites with "hot" (red), "cold" (blue), or "average" (green) electronic coupling to the Cu or heme center given their separation (Eq. 5) in azurin (**C**) and cytochrome c (**D**). Residues in the $\beta$ barrel of azurin are "hot" or "cold" for their distance (depending on whether or not the strand contains a strong connection to the Cu), while those in the $\alpha$-helical region of the protein are weakly coupled for their distance. In cytochrome c, amino acids near the porphyrin axial ligands, the porphyrin covalent bonds to the protein, and the porphyrin hydrogen bonds to the protein are more strongly coupled than expected for their distance. Amino acid numbers are shown.

in the other β strands.

The greater anisotropy of $\zeta_N$ in the secondary structural units of helical proteins compared to β-barrel proteins is also reflected in the larger standard deviation of the fitted value of β/2 (Table 1) for the helical proteins as compared to those of β-barrel structures (*9*). In the β-barrel proteins, a considerably smaller standard deviation is associated with each single (nearly linear) strand that spans the structure from the top of the barrel to the bottom.

Another way to understand the anisotropy of electronic coupling in the helical versus β-barrel proteins is to consider searches from all atoms in the protein to a single probe atom (with the probe not at the Cu or heme site). We have carried out such searches in azurin and myoglobin. In azurin, the fitted value of β/2 is insensitive to the probe atom position when it is in the β-barrel structure (slightly smaller values for β/2 occur for probe atoms near the top or bottom of the barrel and slightly larger values occur for probe atoms near the centers of the strands). This differs from the result in myoglobin, in which β/2 depends on the location of the probe atom in the helix. Even in azurin, if the probe atom is in the helical segment of the protein ($Ala_{60}$ for example), β/2 increases to values typical of the heme proteins. These calculations illustrate that helical and β-barrel motifs differ in both their efficiency and anisotropy as tunneling mediators. The origin of these structural effects lies in the accessibility or inaccessibility of the chosen residue to all other groups through efficient pathways (Fig. 2).

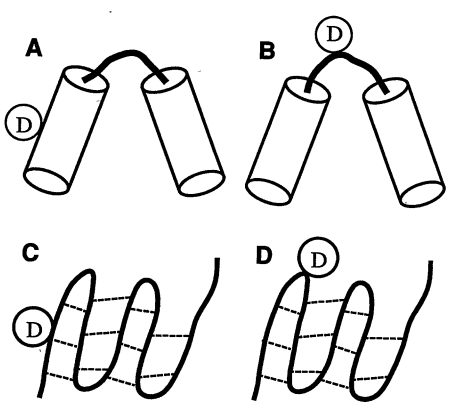


**Fig. 2.** Large differences in average coupling between one probe site (D) and the rest of the protein occur in helical proteins when the probe is at a helix center (**A**) or at a turn between helical regions (**B**) because of the differential accessibility of these sites through strongly coupled pathways. Cylinders represent helical segments of protein. Amino acids at turns are, on average, more strongly coupled to the rest of the protein than those in other positions. Small differences in average coupling are seen in β-barrel proteins for a probe in the middle of a strand (**C**) versus the turn between strands (**D**).

The three-dimensional structure of a protein sets limits on the average decay of the tunneling matrix element in the protein. Simple models give the upper limit of the decay as proportional to the square root of the binding energy of the transferring electron, that is, the decay for tunneling through vacuum. The lower bound on the decay is related to the electronic coupling between neighboring covalent bonds and the tunneling energy relative to the bond energies (*2, 3*). The decay of the coupling matrix element in specific proteins falls between these two values and depends on the secondary and tertiary protein structure. If the unique charge localization site (the Cu, porphyrin, or Fe-S center) is embedded in a highly interconnected β-sheet structure or is at the turn between α-helical chains, it couples more strongly with the protein than if it were embedded in the middle of an α-helical segment. A substantial qualitative difference is seen, therefore, between the average coupling of heme and blue Cu proteins. Moreover, amino acids in β strands directly ligated to the Cu in the β-barrel proteins are predicted to be more strongly coupled than those at a nearly identical distance but on β strands (or helical segments) not coordinating the Cu.

Amino acids exist in electron transfer proteins that are anomalously strongly or weakly coupled ($\zeta_N$ much larger or smaller than 1) for their distance from the charge localization site. Experimental evidence of this behavior was recently reported in ruthenated cytochrome c (*3, 7*). In those experiments, the pathway model accounts for observed rate differences not predicted with simple exponential decay expressions for $T_{DA}$. Differences in the average distance decay of the tunneling matrix element for various proteins should substantially affect observed electron transfer rates because β/2 appears as an exponential contribution. The set of protein pathway couplings that produced the average decay constants in Table 1 were used to produce coupling maps and maps showing anomalously strongly or weakly coupled residues for their distance. Figure 1 shows these maps for cytochrome c and azurin. The coupling maps display the roughly exponential decay of coupling with distance. In the ratio maps (Eq. 5), amino acids predicted to be "hot" ($\zeta_N > 1$) or "cold" ($\zeta_N < 1$) with respect to electron transfer (given their distance) are easily identified. These figures show α-carbons color-coded according to the pathway coupling or $\zeta_N$ value (tubes connecting the α-carbons show the connectivity of the protein and are color-coded according to the value for the α-carbon nearest the COOH-terminus of the protein). The extent to which the protein secondary and tertiary structure provides relatively direct (almost linear) pathways that radiate from the charge localization site to a particular amino acid determines whether it is "hot" or "cold." For example, cytochrome $b_5$ consists of 29% β sheet, but the sheet structure runs in a plane perpendicular to the porphyrin and is not well connected to it, so the average distance decay (Table 1) is close to that of the other highly helical proteins, and no particularly "hot" spots exist in the β-sheet region. The heme in cytochrome $c_{551}$ is the most weakly coupled of all the proteins studied, apparently because of the relatively short and randomly oriented helical segments in the protein.

Improved estimates of $\epsilon^C$ for specific bonds are emerging from quantum chemical calculations (*10*), as are new methods for summing the contributions to $T_{DA}$ from intersecting pathways (*11*). This work should produce more reliable predictions of $T_{DA}$ for proteins. The reported trends in β/2 are expected to be generic because the values of $\epsilon$ and their decay with distance were chosen in a physically reasonable range, and many protein pathways are not highly interconnected.

Bimolecular electron transfer in proteins may be mediated by interactions in a single docking configuration or a family of configurations; in either limit, the pathway model can yield testable predictions of the couplings. One might expect the specificity of electron transfer reactions to be controlled, to some extent, by the structural motifs of the proteins that surround the redox centers. Proteins with different motifs are predicted to display average distance dependencies that are qualitatively different, and the coupling at a given distance is expected to be somewhat anisotropic. The availability of theoretical electronic coupling maps for proteins with known structures should assist in future molecular design projects.

REFERENCES AND NOTES


1. R. A. Marcus and N. Sutin, *Biochim. Biophys. Acta* **811**, 265 (1985); D. DeVault, *Quantum Mechanical Tunneling in Biological Systems* (Cambridge Univ. Press, New York, ed. 2, 1984).
2. J. N. Onuchic and D. N. Beratan, *J. Chem. Phys.* **92**, 722 (1990); D. N. Beratan and J. N. Onuchic, *Photosynth. Res.* **22**, 173 (1989); ———, J. J. Hopfield, *J. Chem. Phys.* **86**, 4488 (1987).
3. D. N. Beratan, J. N. Onuchic, J. N. Betts, B. E. Bowler, H. B. Gray, *J. Am. Chem. Soc.* **112**, 7915 (1990); D. N. Beratan, J. N. Onuchic, H. B. Gray, in *Metal Ions in Biological Systems*, H. Sigel and A. Sigel, Eds. (Dekker, New York, 1991), vol. 27, pp. 97–127.
4. One can calculate the $\epsilon$'s for a physical pathway using perturbation theory, band theory neglecting the influence of side chains, or exact methods for a single physical pathway. Multiple pathways and

interference effects have been considered and appear to be of limited importance when one uses these qualitative arguments.

5. J. J. Hopfield, *Proc. Natl. Acad. Sci. U.S.A.* **71**, 3640 (1974); J. Jortner, *Biochim. Biophys. Acta* **594**, 139 (1980); D. N. Beratan, J. N. Onuchic, J. J. Hopfield, *J. Chem. Phys.* **83**, 5325 (1985); D. N. Beratan and J. J. Hopfield, *J. Am. Chem. Soc.* **106**, 1584 (1984).
6. A. Kuki and P. G. Wolynes, *Science* **236**, 1647 (1987); A. Broo and S. Larsson, *Int. J. Quantum Chem. Quant. Biol. Symp.* **16**, 185 (1989).
7. J. A. Cowan, R. K. Upmacis, D. N. Beratan, J. N. Onuchic, H. B. Gray, *Ann. N.Y. Acad. Sci.* **550**, 68 (1988); B. E. Bowler, T. J. Meade, S. L. Mayo, J. H. Richards, H. B. Gray, *J. Am. Chem. Soc.* **111**, 8757 (1989); M. J. Therien, M. A. Selman, H. B. Gray, I.-J. Chang, J. R. Winkler, *ibid.* **112**, 2420 (1990); S. E. Peterson-Kennedy, J. L. McGourty, J. A. Kalweit, B. M. Hoffman, *ibid.* **108**, 1739 (1986); D. W. Conrad and R. A. Scott, *ibid.* **111**, 3461 (1989); B. Durham, L. P. Pan, J. E. Long, F. Millett, *Biochemistry* **28**, 8659 (1989); O. Farver and I. Pecht, *FEBS Lett.* **244**, 379 (1989); M. P. Jackman, J. McGinnis, R. Powls, G. A. Salmon, A. G. Sykes, *J. Am. Chem. Soc.* **110**, 5880 (1988); B. A. Jacobs *et al.*, *ibid.*, in press.
8. Heteroatom hydrogens were added to the crystallographic coordinates of the other atoms using the software BIOGRAF: BioDesign, Inc., Pasadena, CA 91101.
9. We define the standard deviation of β/2

$$\sigma(\beta/2) = \left\{(1/N)\sum_i \left[\frac{\ln A - \ln \pi_i}{R_i} - \frac{\beta}{2}\right]^2\right\}^{1/2} \quad (6)$$

where $\pi_i$ is the pathway coupling to site $i$ in the protein, which contains $N$ nonhydrogen atoms.
10. V. Balaji, L. Ng, K. D. Jordan, M. N. Paddon-Row, H. K. Patney, *J. Am Chem. Soc.* **109**, 6957 (1987).
11. J. N. Onuchic, P. C. P. Andrade, D. N. Beratan, *J. Chem. Phys.*, in press; C. Goldman, *Phys. Rev. A.* **43**, 4500 (1991).
12. This work was performed in part at the Jet Propulsion Laboratory, California Institute of Technology, and was sponsored by the Department of Energy's Catalysis/Biocatalysis Program (Advanced Industrial Concepts Division) through an agreement with the National Aeronautics and Space Administration. We thank the National Science Foundation and the Conselho Nacional de Des envolvimento Científico e Tecnológico (Brazil) for a binational research grant that allowed international visits during which this work was initiated. Work in San Diego was funded by a research contract from the Jet Propulsion Laboratory, supported by the Department of Energy's Catalysis/Biocatalysis Program and the National Science Foundation (grant DMB-9018768). The pathway search software, written in FORTRAN for Silicon Graphics IRIS computers, is available from D.N.B. at the Beckman Institute address. J.N.O. is in residence at the Instituto de Física e Química de São Carlos, Universidade de São Paulo, 13560, São Carlos, São Paulo, Brazil during the summers.

19 November 1990; accepted 14 March 1991

# Compressibility of Solid $C_{60}$

JOHN E. FISCHER,* PAUL A. HEINEY, ANDREW R. MCGHIE, WILLIAM J. ROMANOW, ARNOLD M. DENENSTEIN, JOHN P. MCCAULEY, JR., AMOS B. SMITH III

**Room-temperature powder x-ray diffraction profiles have been obtained at hydrostatic pressures $P = 0$ and 1.2 gigapascals on the solid phase of cubic $C_{60}$ ("fullerite"). Within experimental error, the linear compressibility $d(\ln a)/dP$ is the same as the interlayer compressibility $d(\ln c)/dP$ of hexagonal graphite, consistent with van der Waals intermolecular bonding. The volume compressibility $-d(\ln V)/dP$ is $7.0 \pm 1 \times 10^{-12}$ square centimeter per dyne, 3 and 40 times the values for graphite and diamond, respectively.**

THE RECENT DISCOVERY OF AN EFFICIENT synthesis of $C_{60}$ and $C_{70}$ has, among other things, facilitated the study of a new class of molecular crystals ("fullerites") based on these molecules ("fullerenes") (*1*). The first x-ray powder diffraction profile of solid $C_{60}$ was analyzed in terms of a faulted hexagonal close-packed (hcp) lattice (*1*), consistent with close packing of spherical molecules but with weak second-neighbor intermolecular interactions. A more recent single-crystal study shows that the molecules are actually centered on sites of an unfaulted face-centered cubic (fcc) Bravais lattice but with a high degree of rotational disorder (*2*). With either indexing, the center-to-center distance between neighboring molecules is 10.0(2) Å, implying a van der Waals (VDW) separation of 2.9 Å for a calculated $C_{60}$ diameter of 7.1 Å (*3*). Nuclear magnetic resonance (NMR) spectroscopy clearly indicates the existence of dynamical disorder (presumably free rotation) which decreases with decreasing temperature (*4, 5*). More work is needed to reconcile conclusions pertaining to dynamic effects on the different time scales of x-ray and NMR experiments.

The nature of intermolecular bonding is of considerable interest, both in its own right and as a clue to the potential electronic properties of fullerites and their derivatives. One expects a priori that the bonding would consist primarily of VDW interactions, analogous to interlayer bonding in graphite. Isothermal compressibility is a sensitive probe of interatomic-intermolecular bonding in all forms of condensed matter and also provides a check on the potentials used in molecular dynamics simulations. We have performed such an experiment on pure solid $C_{60}$, using standard diamond anvil techniques and powder x-ray diffraction. We find that, within experimental error, the linear compressibility $d(\ln a)/dP$ of cubic $C_{60}$ is the same as the $c$-axis or interlayer compressibility $d(\ln c)/dP$ of graphite. This indicates that the functional relations between energy and close-packed layer separation are similar in the two solids.

We used standard techniques to prepare our powder sample: soot production by "burning" graphite rods in 300-torr He, Soxhlet extraction in boiling toluene, and liquid chromatography in hexanes on neutral alumina (*6*). High-performance liquid chromatography (HPLC) with a Pirkle column (*7*) showed >99.5% pure $C_{60}$. The resulting powder was dried in flowing $N_2$ at 400°C to drive off all traces of solvents. Preliminary powder diffraction profiles were consistent with an fcc cell, $a = 14.1$ Å, with no detectable peaks from other phases. A small amount of powder was packed into a hole 1 mm in diameter in a stainless steel gasket 0.6 mm thick, located between the anvils of a standard Merrill-Bassett diamond anvil cell (DAC). A hydrostatic environment was assured by filling the remaining volume with a 50:50 mixture of ethanol: methanol. Attempts to incorporate a small amount of powdered solid with known compressibility along with the fullerite were unsuccessful; after several tries, we were unable to produce a usable combination of relative scattering intensities, clearly defined peaks, and measurable pressure shifts using any of the usual standards. Thus we resorted to a secondary pressure scale based on the torque of the three screws that compress the liquid and deform the gasket (as established in previous experiments). After measuring the fullerite at "high" pressure, we reloaded the cell with graphite powder, using an identical gasket, and measured the position of the graphite (002) reflection at the same torque settings used for the fullerite measurements. This procedure established that the torque-pressure relation conformed to the secondary standard to within 10%.

J. E. Fischer, Laboratory for Research on the Structure of Matter and Department of Materials Science and Engineering, University of Pennsylvania, Philadelphia, PA 19104.
P.-A. Heiney and A. M. Denenstein, Laboratory for Research on the Structure of Matter and Department of Physics, University of Pennsylvania, Philadelphia, PA 19104.
A. R. McGhie and W. J. Romanow, Laboratory for Research on the Structure of Matter, University of Pennsylvania, Philadelphia, PA 19104.
J. P. McCauley, Jr., and A. B. Smith III, Laboratory for Research on the Structure of Matter and Department of Chemistry, University of Pennsylvania, Philadelphia, PA 19104.

*To whom correspondence should be addressed at the Department of Materials Science and Engineering.